Supporting Information

First-principles study on the interplay of strain and state-of-charge with Li-ion diffusion in the battery cathode material $LiCoO_2$

Zizhen Zhou,[a, b,] Claudio Cazorla,[c] Bo Gao,[b, d] Huu Duc Luong,[b] Toshiyuki Momma[a] and Yoshitaka Tateyama[a,b,e,*]*

a, Graduate School of Advanced Science and Engineering, Waseda University, 3-4-1, Okubo, Shinjuku-ku, Tokyo 169-8555, Japan

b, Research Center for Energy and Environmental Materials (GREEN), National Institute for Materials Science (NIMS), 1-1 Namiki, Tsukuba, Ibaraki 305-0044, Japan

c, Departament de Física, Universitat Politècnica de Catalunya, Campus Nord B4-B5, E-08034 Barcelona, Spain

d, College of Materials Science and Engineering, Jilin University, Changchun, Jilin 130012, People's Republic of China

e, Laboratory for Chemistry and Life Science, Tokyo Institute of Technology, 4259 Nagatsuta-cho, Midori-ku, Yokohama 226-8503, Japan

* Corresponding Author: zizhen_zhou@toki.waseda.jp; tateyama.yoshitaka@nims.go.jp

KEYWORDS: biaxial strain, hydrostatic pressure, layered cathode material, ionic diffusion, vacancy.

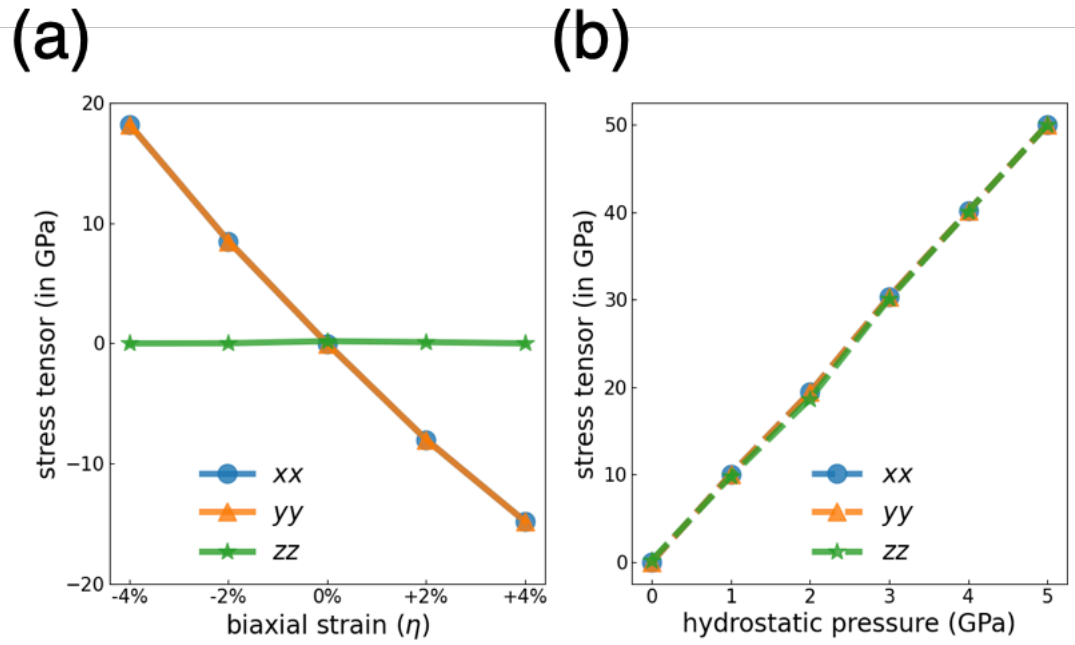

Figure S1. Stress tensor components of *xx*, *yy* and *zz* for $LiCoO_2$ as a function of (a) the biaxial strain *η* and (b) hydrostatic pressure.

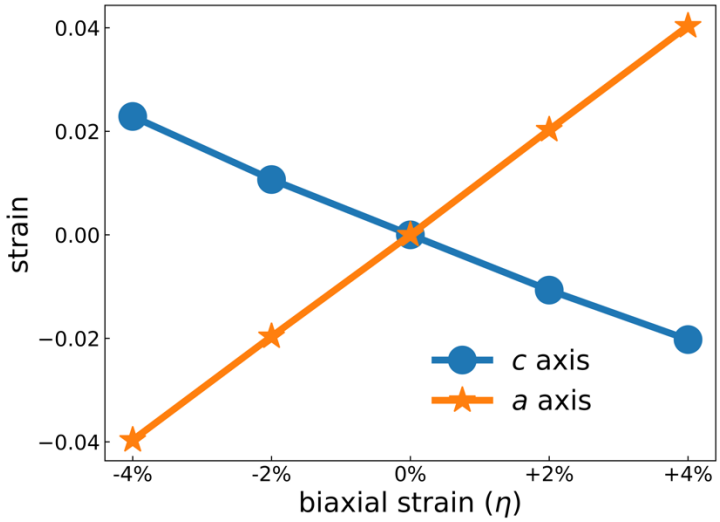

Figure S2. Strain along the *a* and *c* axes for $LiCoO_2$ as a function of biaxial strain (η).

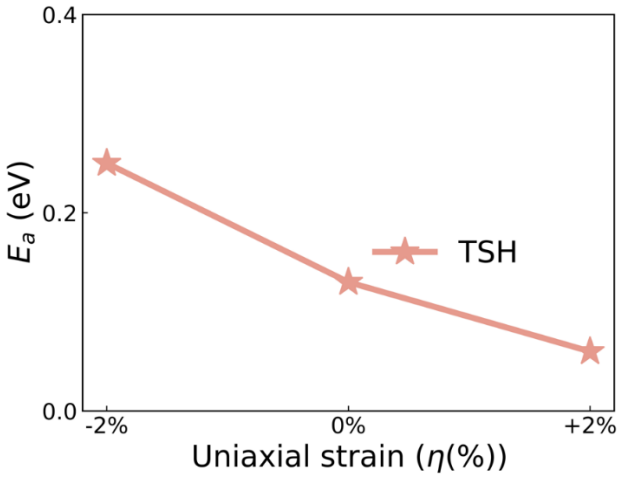

Figure S3. NEB migration energy barrier (E_a) results of LCO expressed as a function of uniaxial strain along the *c* axis for the TSH diffusion mechanism, where positive (negative) ratio corresponds to tensile (compressive) strain.

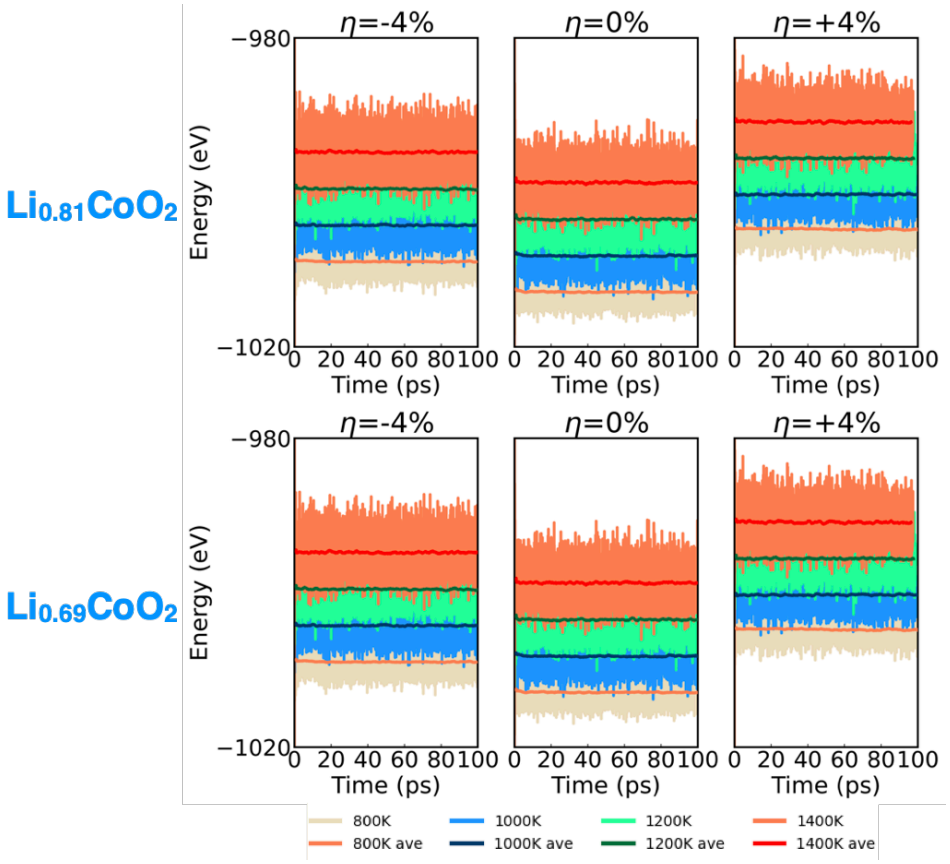

Figure S4. Energy evolutions and corresponding energies averaged over 100,000 steps in the FPMD simulations of LCO under η=-4%, 0%, +4% at 800, 1000, 1200 and 1400 K. Upper panels: $Li_{0.81}CoO_2$. Lower panels: $Li_{0.69}CoO_2$.

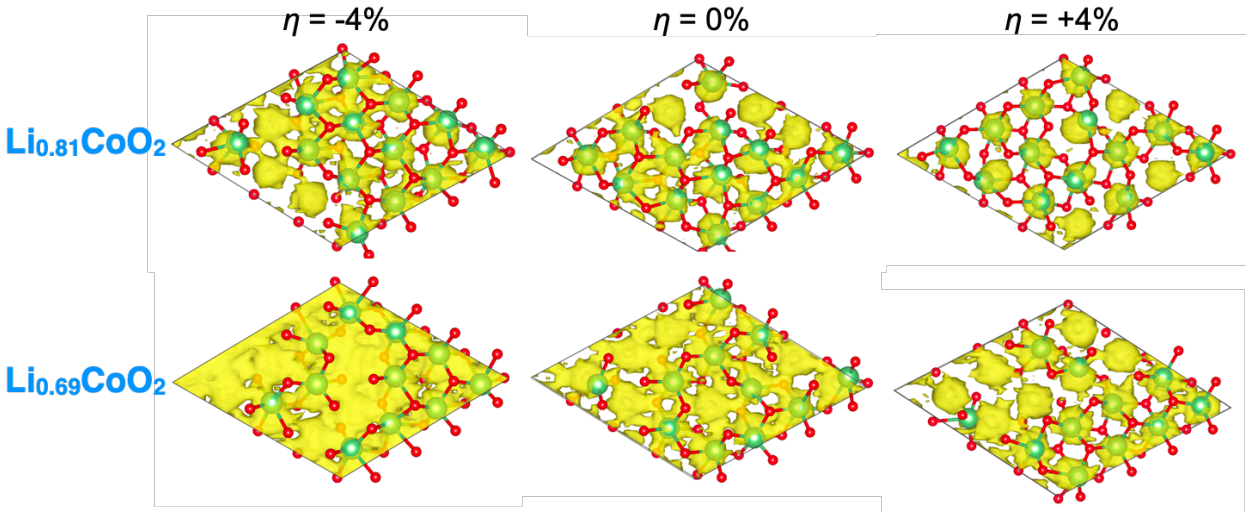

Figure S5. Li^+ trajectory densities for one Li layer in $LiCoO_2$ accumulated from 20 to 100 ps in the FPMD simulations for η=-4%, 0% and +4% at 1200 K. Upper panel represents structures for $Li_{0.81}CoO_2$. Lower panel represents structures for $Li_{0.69}CoO_2$.

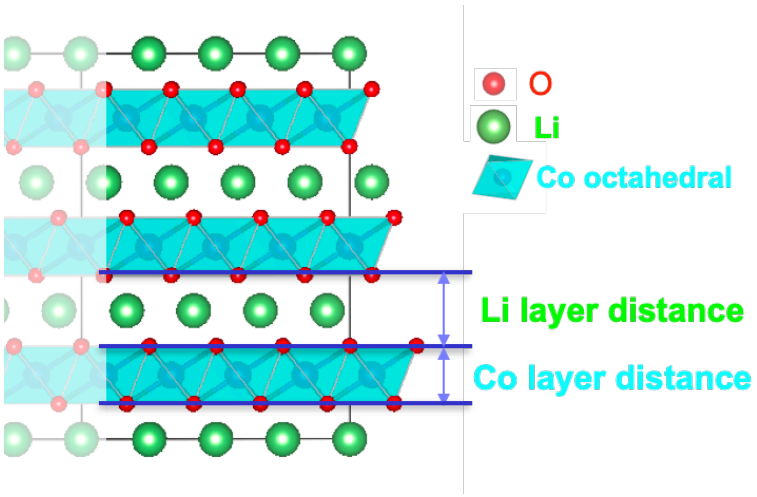

Figure S6. Schematic picture of the defined "Co layer distance" and "Li layer distance".

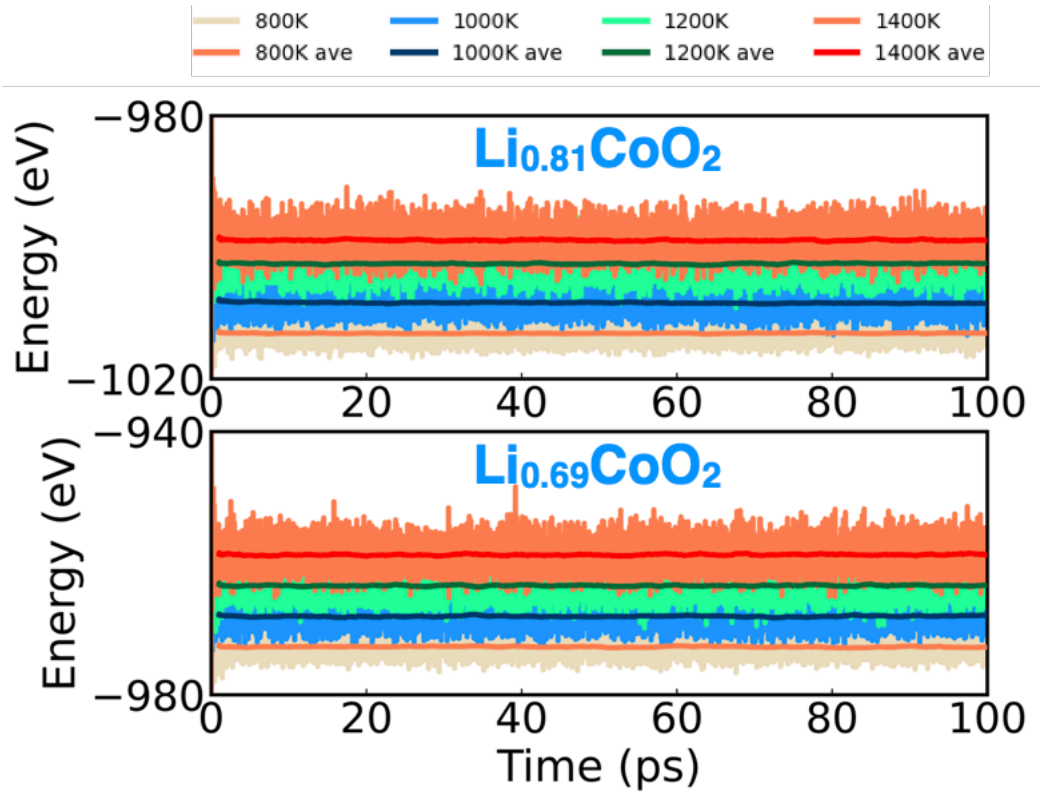

Figure S7. Energy evolutions and corresponding energies averaged over 100,000 steps in the FPMD simulations of LCO under a hydrostatic pressure ~1 GPa at 800, 1000, 1200 and 1400 K. Upper panel: $Li_{0.81}CoO_2$. Lower panel: $Li_{0.69}CoO_2$.

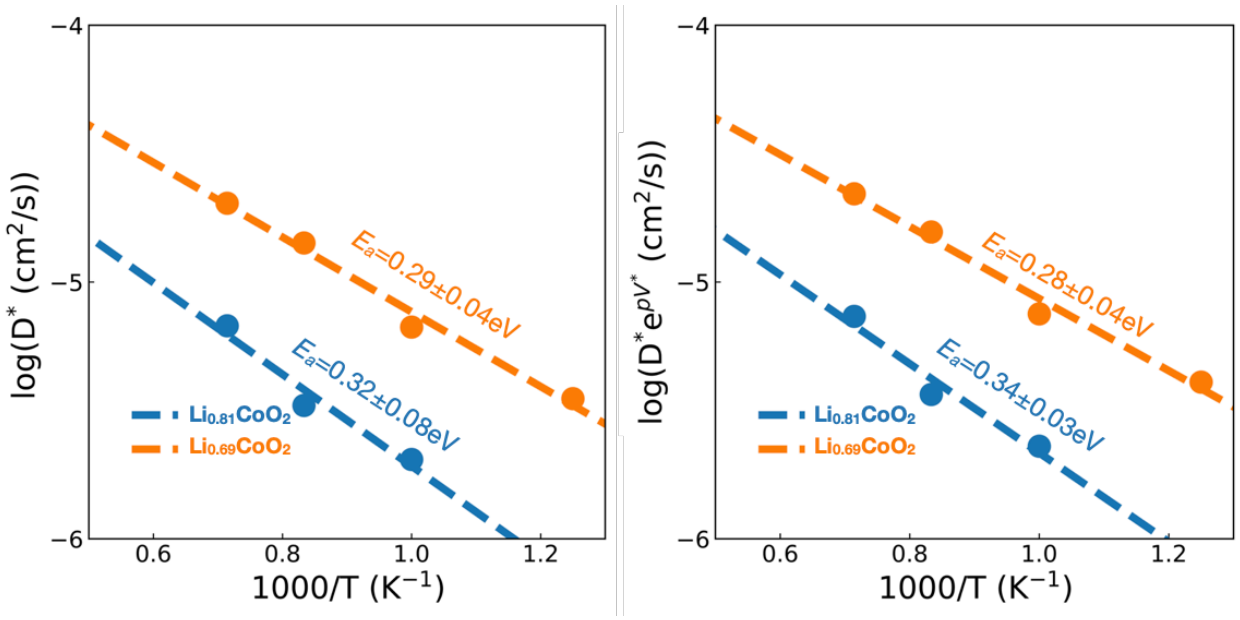

Figure S8. Arrhenius plot comparison for LCO under ~1 GPa hydrostatic pressure of one-step fitting (left panel) and two-step fitting (right panel). *p* stands for hydrostatic pressure, V^* stands for the V_a obtained from NEB calculations.

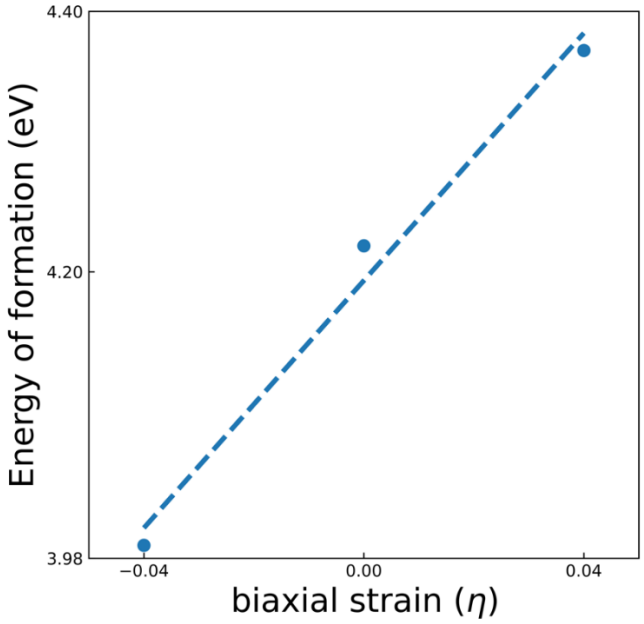

Figure S9. The energy of formation of a Li vacancy at biaxial strain η where η=-4%, 0%, +4%.

Table S1

(a). Lattice parameters *a* and *c* for $LiCoO_2$, $Li_{0.81}CoO_2$ and $Li_{0.69}CoO_2$ under external biaxial strain.

a	η=-4%	η=0%	η=+4%
$LiCoO_2$	2.71 Å	2.82 Å	2.93 Å
$Li_{0.81}CoO_2$	2.70 Å	2.82 Å	2.93 Å
$Li_{0.69}CoO_2$	2.70 Å	2.81 Å	2.92 Å

c	η=-4%	η=0%	η=+4%
$LiCoO_2$	14.46 Å	14.15 Å	13.87 Å
$Li_{0.81}CoO_2$	14.52 Å	14.19 Å	13.90 Å
$Li_{0.69}CoO_2$	14.60 Å	14.25 Å	13.94 Å

(b). Lattice parameters *a* and *c* for $LiCoO_2$ under external uniaxial strain.

	η=-2%	η=+2%
a	2.83 Å	2.81 Å
c	13.85 Å	14.42 Å

Table S2. Diffusion coefficients at 300 K for $Li_{0.81}CoO_2$ and $Li_{0.69}CoO_2$ under external biaxial strain.

	η=-4%	η=0%	η=+4%
$Li_{0.81}CoO_2$	6.2×10^{-9} cm^2/s	5.3×10^{-9} cm^2/s	6.0×10^{-12} cm^2/s
$Li_{0.69}CoO_2$	3.9×10^{-8} cm^2/s	4.2×10^{-9} cm^2/s	3.8×10^{-10} cm^2/s

Table S3. Li layer distances for $Li_{0.81}CoO_2$ and $Li_{0.69}CoO_2$ under external biaxial strain.

$Li_{0.81}CoO_2$	Li layer distance
η=-4%	2.71 Å
η=0%	2.69 Å
η=+4%	2.67 Å

$Li_{0.69}CoO_2$	Li layer distance
η=-4%	2.77 Å
η=0%	2.76 Å
η=+4%	2.76 Å

Table S4. Lattice parameters *a* and c for $Li_{0.81}CoO_2$ and $Li_{0.69}CoO_2$ under hydrostatic pressure (1 GPa). Strain (η) along *a, b* and *c* are calculated with respect to the original lattice parameters, reported in Table S1 (a).

	a	η	*c*	η
$Li_{0.81}CoO_2$	2.811 Å	-0.2%	14.128 Å	-0.4%
$Li_{0.69}CoO_2$	2.805 Å	-0.2%	14.165 Å	-0.6%

Table S5. Li and Co layer distances for $Li_{0.81}CoO_2$ and $Li_{0.69}CoO_2$ under a hydrostatic pressure of ~1 GPa.

	Li layer distance	Co layer distance
$Li_{0.81}CoO_2$	2.67 Å	2.04 Å
$Li_{0.69}CoO_2$	2.74 Å	2.00 Å

Table S6. Lattice parameters *a* and *c*, activation energy (E_a) along TSH pathway for $LiCoO_2$ under a hydrostatic pressure of 1~5 GPa. Strain (η) along *a, b* and *c* are calculated with respect to the original lattice parameters, reported in Table S1 (a).

hydrostatic pressure	*a*	η	*c*	η	E_a
1 GPa	2.820 Å	-0.21%	14.109 Å	-0.29%	0.22 eV
2 GPa	2.815 Å	-0.39%	14.057 Å	-0.66%	0.24 eV
3 GPa	2.810 Å	-0.57%	14.016 Å	-0.95%	0.26 eV
4 GPa	2.806 Å	-0.71%	13.961 Å	-1.34%	0.29 eV
5 GPa	2.802 Å	-0.85%	13.923 Å	-1.60%	0.32 eV

Table S7. Number of electrons transferred from Li in LCO under external biaxial strain.

η=-4%	η=0%	η=+4%
0.886	0.891	0.895

Table S8. Bandgap of fully lithiated LCO under biaxial strain and hydrostatic pressure.

	Bandgap (eV)
η=-4%	2.52
η=0%	2.75
η=+4%	2.89
hydrostatic pressure	2.76

Table S9. Effective mass of LCO under biaxial strain.

	Effective mass (m_e)
η=-4%	-0.80
η=0%	-0.74
η=+4%	-0.67

Supporting Discussion 1

The interaction between stoichiometric LCO electronic structure and biaxial strain is analysed. The partial density of electronic states (DOS) calculated for the LCO under biaxial strain is shown in Figure S10. It is noticeable that the bandgap decreased by ~0.2 eV under η=-4% whereas it increased (~1.5 eV) under η=+4%. This can be understood by the reduced (enlarged) interatomic distance for the compressive (tensile) strain side, which leads to an increase (decrease) in the crystal field and consequent enlargement (reduction) of the energy difference between the corresponding bonding and antibonding electronic states.[1] Specifically, in the case of η=-4%, Li-O bond length was shortened from 2.07 Å to 2.02 Å and Co-O bond length from 1.92 Å to 1.89 Å. A similar bandgap variation with respect to the bond length was also reported by Jun *et al*.[2] However, the bandgap of LCO under a hydrostatic pressure ~1 GPa does not change much (See Table S8). This could be ascribed to the barely changed lattice parameters (*a*, *b* and *c* decrease less than 0.02%).

To comprehensively evaluate the electronic properties, we have introduced the calculation of the effective mass (shown in Table S9). Our results indicate that LCO under compressive strain (η=-4%) exhibits a more negative effective mass compared to LCO under tensile strain (η=+4%), suggesting a reduction in carrier mobility under biaxial compressive strain, whereas an enhancement is anticipated under biaxial tensile strain.[3, 4] To gain deeper insights, we extended our investigation to delithiated LCO, thereby exploring the impact of biaxial strain and hydrostatic pressure on electrical conductivity. $Li_{0.69}CoO_2$ is selected as an example and band structures of it under biaxial strain and hydrostatic pressure are shown in Figure S11. The electronic conductivity is obtained using the semiclassical Boltzmann transport equations (BTE) implemented via BOLTZTRAP2 code.[5] Transport tensors as a function of the chemical potential μ can be expressed by:

$$[\sigma]_{ij}(\mu, T) = e^2 \int_{+\infty}^{+\infty} dE \left(-\frac{\partial f(E, \mu, T)}{\partial E} \right) \Sigma_{ij}(E) \qquad \text{(S1)}$$

where the first term $f(E, \mu, T)$ stands for the Fermi-Dirac distribution function with respect to the energy $f(E, \mu, T) = \frac{1}{e^{(\varepsilon_i - \mu)/k_B T} + 1}$.

The second term represents the transport distribution function, which is defined by:

$$\Sigma_{ij}(E) = \frac{1}{V}\sum_{n,k} v_i(n,k) v_j(n,k) \tau_{n,k} \delta(E - E_{n,k}) \quad \text{(S2)}$$

$E_{n,k}$ is the energy for band n at k; v_i is the i-th and v_j the j-th component of the band velocity at (n, k). τ is the lifetime for an electron on band n at wave vector k. We selected 1 fs in this work.[3]

The simulated electrical conductivity for $Li_{0.69}CoO_2$ at η=0% aligns reasonably well with experimental outcomes, as illustrated in Figure S12.[6] Notably, at η=-4%, the electrical conductivity diminishes between 200 K and 500 K, whilst a minor elevation is observed at η=+4% and under hydrostatic pressure. These observations align coherently with our analysis of the pristine LCO.

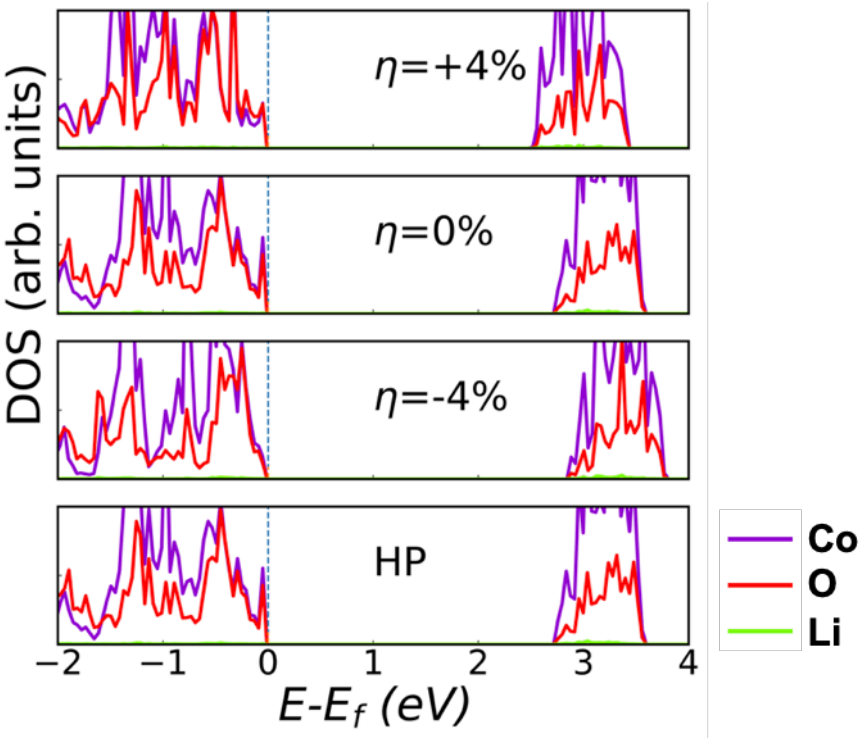

Figure S10. Partial DOS calculated for $LiCoO_2$ under a hydrostatic pressure of ~1 GPa and biaxial strains of -4%, 0%, and +4%. Blue dotted lines indicate the fermi energy.

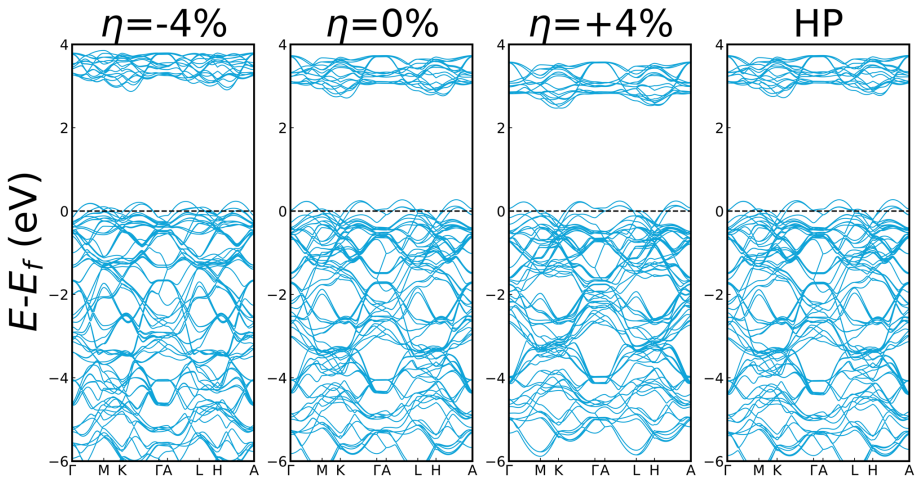

Figure S11. Band structure plot for $Li_{0.69}CoO_2$ under biaxial strain and hydrostatic pressure (HP).

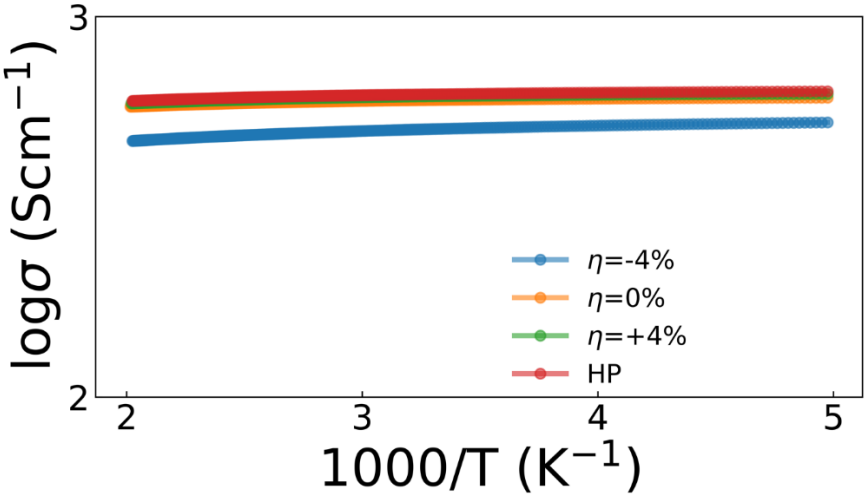

Figure S12. Estimated temperature dependence of electrical conductivity for $Li_{0.69}CoO_2$ under biaxial strain and hydrostatic pressure (HP).

Supporting Discussion 2

The change of total energy of the system $\boldsymbol{\Delta E}$ under strain can be expressed as:

$$\boldsymbol{\Delta E} = \frac{\mathbf{1}}{\mathbf{2}} \boldsymbol{V_0} \sum_{\boldsymbol{ijkl}} \boldsymbol{C_{ijkl} \varepsilon_{ij} \varepsilon_{kl}} \tag{S3}$$

where V_0 is the original volume without any strain, C_{ijkl} is the elastic stiffness tensor and $\boldsymbol{\varepsilon_{ij}}$ is the strain on the system.

$$\frac{\boldsymbol{\partial E}}{\boldsymbol{\partial \sigma_{ij}}} = \boldsymbol{V_0} \sum_{\boldsymbol{kl}} \boldsymbol{C^{-1}_{ijkl} \varepsilon_{kl}} = \boldsymbol{V_0 \varepsilon_{ij}} \tag{S4}$$

By swapping:

$\boldsymbol{E \rightarrow E_a}$ and $\boldsymbol{V_0 \varepsilon_{ij} \rightarrow V_{a\,ij}}$, the equation (S4) can be expressed as:

$$\boldsymbol{V_{a\,ij}} = \frac{\boldsymbol{\partial E_a}}{\boldsymbol{\partial \sigma_{ij}}} \tag{S5}$$

Since LCO is under hydrostatic pressure, in which $\boldsymbol{\sigma_{11} = \sigma_{22} = \sigma_{33}}$, Equation (5) in the main text can be written in Equation (S6),

$$\boldsymbol{V_{a\,ij}} = \frac{\boldsymbol{\partial E_a}}{\boldsymbol{C_{ijkl} \partial \varepsilon_{ij}}} = \boldsymbol{C^{-1}_{ijkl}} \frac{\boldsymbol{\partial E_a}}{\boldsymbol{\partial \varepsilon_{ij}}} \tag{S6}$$

where calculated $\boldsymbol{\varepsilon_{ij}}$ and C_{ijkl} [GPa] excluding the shear components are:

$$\boldsymbol{\varepsilon_{ij}} = \begin{bmatrix} \mathbf{0.0085} & \mathbf{0} & \mathbf{0} \\ \mathbf{0} & \mathbf{0.0085} & \mathbf{0} \\ \mathbf{0} & \mathbf{0} & \mathbf{0.016} \end{bmatrix} \qquad \boldsymbol{C_{ijkl}}\ \mathbf{[GPa]} = \begin{bmatrix} \mathbf{351} & \mathbf{92} & \mathbf{60} \\ \mathbf{92} & \mathbf{351} & \mathbf{60} \\ \mathbf{60} & \mathbf{60} & \mathbf{227} \end{bmatrix}$$

Note that and C_{ijkl} [GPa] is in good agreement with previous calculation.[7] Then the $V_{a\,ij}$ [cm^3/mol] in its tensor form is expressed as:

$$\boldsymbol{V_{a\,ij}\ [cm^3/mol]} = \begin{bmatrix} \mathbf{2.85} & \mathbf{0} & \mathbf{0} \\ \mathbf{0} & \mathbf{2.85} & \mathbf{0} \\ \mathbf{0} & \mathbf{0} & \mathbf{2.28} \end{bmatrix}$$

References

(1) Liu, Z.; Menéndez, C.; Shenoy, J.; Hart, J. N.; Sorrell, C. C.; Cazorla, C. Strain Engineering of Oxide Thin Films for Photocatalytic Applications. *Nano Energy* **2020**, *72*, 104732.

(2) Cao, J.; Chen, Z.; Zhong, R.; Zhang, Y.; Ding, Q.; Li, H. Study on the Performance of Different Valence Cations Doped into $LiCoO_2$ Cathode for Li-Ion Batteries. *Journal of Electronic Materials* **2021**, *50* (11), 6386-6391.

(3) Luong, H. D.; Xu, C.; Jalem, R.; Tateyama, Y. Evaluation of Battery Positive-Electrode Performance with Simultaneous *Ab-Initio* Calculations of Both Electronic and Ionic Conductivities. *Journal of Power Sources* **2023**, *569*, 232969.

(4) Tsymbalov, E.; Shi, Z.; Dao, M.; Suresh, S.; Li, J.; Shapeev, A. Machine Learning for Deep Elastic Strain Engineering of Semiconductor Electronic Band Structure and Effective Mass. *npj Computational Materials* **2021**, *7* (1), 76.

(5) Madsen, G. K.; Carrete, J.; Verstraete, M. J. Boltztrap2, a Program for Interpolating Band Structures and Calculating Semi-Classical Transport Coefficients. *Computer Physics Communications* **2018**, *231*, 140-145.

(6) Milewska, A.; Świerczek, K.; Tobola, J.; Boudoire, F.; Hu, Y.; Bora, D.; Mun, B.; Braun, A.; Molenda, J. The Nature of the Nonmetal–Metal Transition in Li_xCoO_2 Oxide. *Solid State Ionics* **2014**, *263*, 110-118.

(7) Qi, Y., Hector, L. G., James, C., & Kim, K. J. Lithium concentration dependent elastic properties of battery electrode materials from first principles calculations. *Journal of the Electrochemical Society* **2014**, *161*(11), F3010.